



# City Research Online

## City St George's, University of London

**Citation:** Psyrras, G., Tsavdaridis, K. & Lawson, R. M. (2025). Numerical Investigation of the End-Post Behaviour of Cellular Beams. Paper presented at the The 2nd International Symposium on Advanced Materials and Design for Structural Safety and Sustainability, 6-7 Feb 2025, Lyon, France.

This is the accepted version of the paper.

This version of the publication may differ from the final published version. To cite this item please consult the publisher's version.

**Permanent repository link:** <https://openaccess.city.ac.uk/id/eprint/35098/>

**Copyright and Reuse:** Copyright and Moral Rights remain with the author(s) and/or copyright holders. Copies of full items can be used for personal research or study, educational, or not-for-profit purposes without prior permission or charge, unless otherwise indicated, provided that the authors, title and full bibliographic details are credited, a hyperlink and/or URL is given for the original metadata page and the content is not changed in any way. For full details of reuse please refer to [City Research Online policy](#).

---

# NUMERICAL INVESTIGATION OF THE END-POST BEHAVIOUR OF CELLULAR BEAMS

Georgios Psyrras<sup>1</sup>, Konstantinos Daniel Tsavdaridis<sup>2</sup>, R. Mark Lawson<sup>3</sup>

<sup>1</sup>Georgios Psyrras (City St George's, University of London, Northampton Square, London EC1V 0HB, UK, [giorgos.psyrras@city.ac.uk](mailto:giorgos.psyrras@city.ac.uk))

<sup>2</sup>Konstantinos Daniel Tsavdaridis (City St George's, University of London, Northampton Square, London EC1V 0HB, UK, [konstantinos.tsavdaridis@city.ac.uk](mailto:konstantinos.tsavdaridis@city.ac.uk))

<sup>3</sup>R. Mark Lawson (The Steel Construction Institute, Silwood Park, SL5 7QN, Ascot, UK, [m.lawson@steel-sci.com](mailto:m.lawson@steel-sci.com))

---

**SUMMARY:** *The end-post, the solid web region between the end of the beam and the first web opening, is treated in a similar manner to the beam's web-post in lack of definitive design guidance. However, its behaviour may vary depending on the adjacent connection type and the beam's end configurations. This paper explores in detail the end-post behaviour of cellular beams, focusing on its failure modes and shear resistance. Building upon the experimental work by Tsavdaridis et al. (2024), three cellular beam setups were modelled and analysed using the FE software Abaqus. The FE modelling is discussed. Various end-post configurations were examined through a comprehensive parametric study. The FE analysis results, in agreement with the experimental results, yielded significantly higher failure loads than the design estimates given by Eurocode 3 Part 1-13. The stress distribution plots revealed the high stress concentrations at the vicinity of the first opening that initiated each failure mode. The connection type and the presence of notches or infill plates proved to dictate the stress distribution, ultimately controlling the failure mode.*

**KEY WORDS:** *cellular beams, end-post, failure mode, shear resistance, buckling, finite element analysis*

---

## 1. INTRODUCTION

Cellular beams with large web openings have been widely used in long span steel and composite construction over 30 years. The presence of large web openings introduces many potential failure mechanisms, compared to solid-web beams [4]. Publications including SCI P100 [14], SCI P355 [9], AISC Guides [7] and the recently published Eurocode 3 – Part 13 [2] have addressed the complex behaviours of these structural members and provide guidance on their structural design. BS EN 1993-1-13 gives guidance on the design of end-posts which is an adaptation of the method used for web-post buckling. Numerous studies have been conducted on perforated beams, including cellular beams, the majority of them focusing on addressing the web-post buckling and Vierendeel bending failure modes. Those intricate failure modes are considered the most common failures in practical use cases.

The Vierendeel mechanism, first reported by Altifillisch et al. [1] for castellated beams and later by Redwood and McCutcheon (1968) for cellular beams, is associated with high shear forces that cause the formation of four 'plastic' hinges around the web opening. Redwood [10] and Ward [14] developed simplified analytical linear methods to estimate the Vierendeel bending action in cellular beams. To address the deficiencies of the analytical methods, Chung et al. [3][4] utilised non-linear FEA to develop shear/moment interaction design curves for the Vierendeel failure. Regarding the web-post behaviour, comprehensive research works have been presented by Tsavdaridis and D'Mello [13] and Grilo et al. [8], both involving experimental tests and non-linear FEA with focus on the web-post buckling failure and the prediction of the web-post shear resistance.

In contrast, research on the end-post behaviour next to connections is limited. An end-post is defined as the part of the solid web between the web opening of perforated (cellular) beams and the end

connections to the columns or beams. When the end-post width,  $s_e$ , fulfils  $s_e \geq 0.5s_o$ , where  $s_o$  is the width of the web-post, it was previously assumed that the end-post is not as critical as the first web-post, but this may not be the case because of the different conditions at the connections as well as fabrication methods. In the Eurocode 3 - Part 13 [2] the minimum width of the end-post for circular web openings is given as  $s_e \geq 0.25h_o$  for simply supported beams and  $s_e \geq h_o$  for beams with rigid or semi-rigid connections, where  $h_o$  is the web opening diameter. When the end-post width requirements are not met, an additional infill plate should be welded in the first opening. Depending on the loading conditions, the infill plate can be in the form of a half-infill up to the centreline of the opening or a full infill.

In practice, the connection type adjacent to the end-post might vary greatly and so the connection affects the end-post behaviour. Moreover, notches to the cellular beam flanges are often required at beam-to-beam connections. Notches cause increased stress concentration in the narrow web between the notch and the opening. Regarding their limiting dimensions, no guideline provides recommendations for cellular beams.

Tsavdaridis et al. [12] investigated whether the design approach proposed in Eurocode 3 Part 1-13 [2] could be verified and improved. In a series of tests on cellular beam-to-column connections, the failure modes of the end-posts and the effect of the connections were determined. Three cellular beams of 560 mm depth with 400 mm diameter openings were tested with either bolted fin-plate and end-plate connections at the beam ends. The tested specimens included a narrow end-post beam, an identical narrow end-post beam with notched flanges and a third similar cellular beam with infill plates and notched flanges. The test failure loads were compared to the end-post buckling resistances given in the Eurocode 3 Part 1-13 [2] and exceeded the predicted resistances by 35% to 83%.

## 2. CELLULAR BEAM TESTS ON CONNECTIONS

The following three 3.62 m long cellular beams were tested, based on practical end-post configurations:

- Beam with narrow end-post of 90mm width ( $s_e = 0.225h_o$ ).
- Beam with narrow end-post ( $s_e = 0.225h_o$ ) and notched flanges (90mm wide x 60mm deep notches with a 20mm radius corner).
- Beam with notched flanges (90mm wide x 60mm deep notches with a 20mm radius corner) and 200mm wide half-infill plate of 8mm nominal thickness, forming an end-post of 203mm width.

Each beam had a fin-plate connection on one side and an end-plate connection on the other to enable a direct comparison of their behaviour to be made. The test cellular beams were selected to be indicative of current practice and used 406 x 178 x 67 kg/m UB sections that were cut and re-welded to create a cellular beam of depth  $h = 560$ mm and opening diameter  $h_o = 400$ mm (with  $h_o = 0.71h$ ). The 1m high columns used 203 x 203 x 60 kg/m UC sections. S355 nominal steel grade was used for both beams and columns. Conducting two tests on each one of the three beams allowed for the straightforward comparison of the two connection types and their effect on the failure loads of the end-posts. Two jacks positioned 803mm from either end of the beam applied the incremental load to the beams. Web stiffeners and full infill plates were used at those locations and the beams were laterally restrained at mid-span. For further details, please refer to [12].

## 3. FE VALIDATION OF THE CELLULAR BEAM TESTS

### 3.1. FE Modelling of the Tests

The cellular beam tests on connections presented in [12] were modelled and analysed using the FEA software Abaqus CAE [6]. Several simplifications were made during modelling to analyse the FE models efficiently.

The loads were applied directly to the beams over an area given by the load cells. The column base plate restraints and the lateral torsional buckling restraint were not modelled, instead boundary conditions were applied directly to the base of the columns and to the beam flanges respectively. The column bases are taken as pinned. All tests were modelled as 3D planar shell parts, as shown in Figure 1.

A bilinear stress-strain curve was used to model the steel material behaviour. The values of the steel's yield strength,  $f_y$ , and ultimate strength,  $f_u$ , were provided through mill test certificates by the supplier. The beam stiffeners, the end-plates and the fin-plates were all modelled using their material properties.

**Table 1.** Material properties of steel specimens.

	E	$\nu$	$f_y$	$f_u$	$\epsilon_u$
<b>Beams</b>	200 GPa	0.3	393 MPa	470 MPa	0.20
<b>Columns</b>	200 GPa	0.3	398 MPa	550 MPa	0.20
<b>Infill Plates</b>	200 GPa	0.3	469 MPa	600 MPa	0.20

To accurately mesh the three models a combination of 4-node reduced integration shell elements (S4R) and 3-node reduced integration shell elements (S3) were utilised. Four mesh seed sizes were examined in a mesh convergence study by comparing the applied load versus mid-span deflection curve to the respective test curve. Densely meshed models with seed size of approximately 7.5mm captured well the test behaviour, thus those were selected for the analyses.

Node-to-surface 'Tie' constraints tying all degrees of freedom (DOFs) were used to model the weld connections between the fin-plates and the universal columns, as well the ones between the end-plates and the beams. The bolted connections were modelled using rigid beam constraints, ensuring that there would be no failure in the M20 bolts, as was the case in the tests. Finally, kinematic coupling constraints were used to model the lab tests' jacks and distribute the load uniformly across the width of the top flange.

As part of the modelling simplifications, pinned supports conditions ( $U1=U2=U3=0$ ) were assigned at the bases of the columns, constraining all translational DOFs. In addition, the beam flanges at the mid-span of the beam were restrained laterally ( $U3=0$ ), to model the lateral buckling restraint in the test (see Figure 1). Regarding the loading, two concentrated loads were applied, one at each reference point. The values of the concentrated loads varied depending on the type of the analysis.

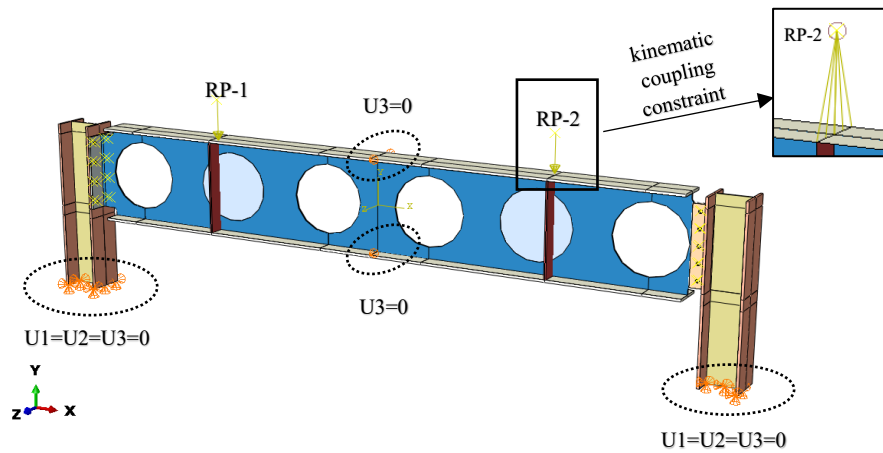


**Figure 1.** Boundary conditions and loads on Test 2 model. Identical conditions were applied to all models.

Two different types of analyses were carried out for this study:

- Geometrically and materially nonlinear static analyses with imperfections (GMNIA) using the Abaqus Standard Solver and Static Riks method, which can predict the response of the specimen until the first beam failure. Two reference loads were used in this case as required by the solver [5].
- Pseudo-static analyses using the Abaqus Explicit Solver, which can simulate the whole loading test procedure, including the second beam failure. Two loads were used in this case, with amplitudes replicating the load protocol that was implemented throughout the lab tests [12].

In both cases, early analyses showed that initial two loading and unloading steps did not affect at all the outcome of the analyses, and they could be ignored.

### 3.2 FE Analyses Results

In this section, the results from FE analyses are discussed and compared to the lab test results. The differences between the Explicit Solver and the Standard Solver model analyses were minor. Both solutions returned similar load – displacement curves and agreed on the first beam failure mode and load. As the Riks analysis (Standard Solver) could not be used to model the full loading procedure, only the Explicit Solver analyses are discussed in the following subsections.

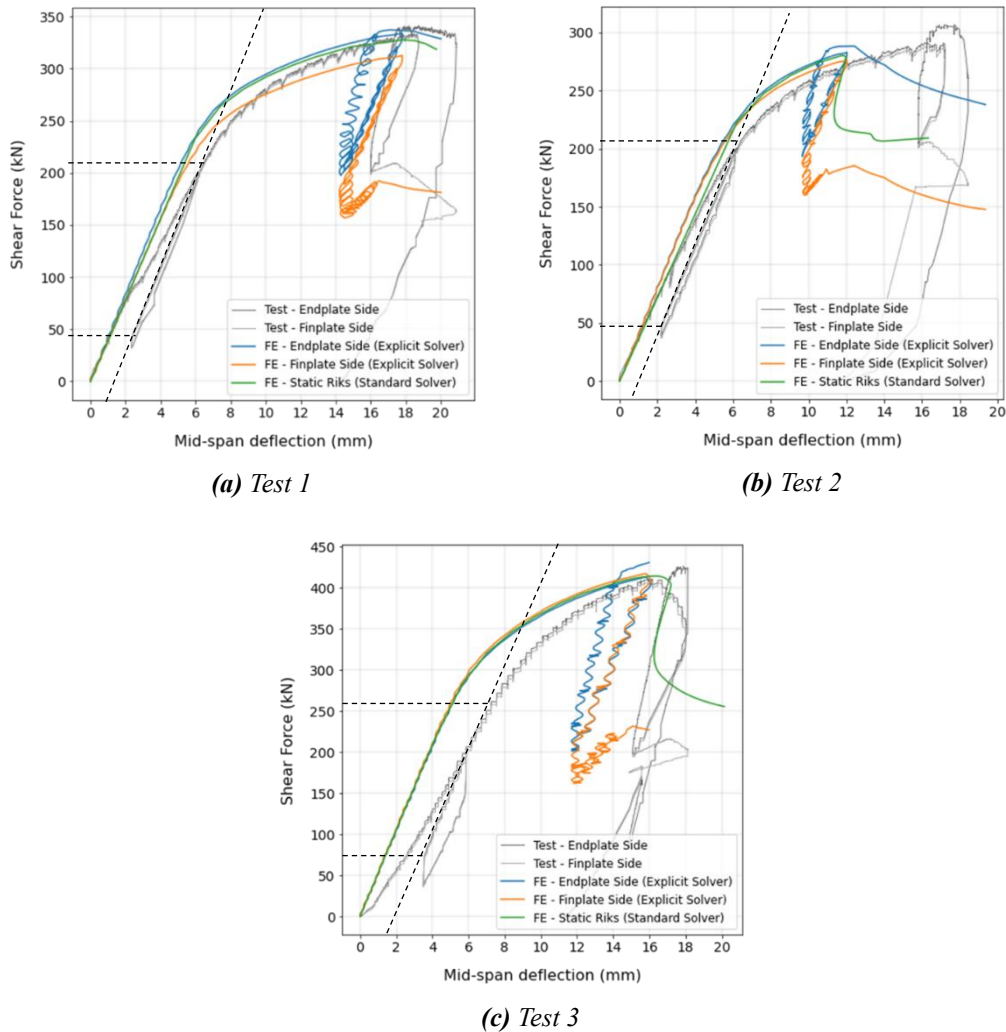


**Figure 2.** Shear force vs. Mid-span vertical deflection curves for the three tests.

The shear force versus mid-span vertical displacement curves are presented in Figure 2; the vertical axes represent the shear forces on both ends of the beam, next to the connections - plotted against the mid-span vertical displacements ( $U_2$ ) as measured at the bottom of the beams. It is evident from the test curves that there was some bolt slippage during the initial loading and unloading, especially for Test 1 and Test 3. This is indicated by the different stiffness slopes during loading steps 1-3 (Figure 2a, 2c) between test and FE results, while the frame's behaviour was elastic. The actual stiffness of the tested frames, after the bolts bore into the bolt holes, equals to the slope of the black dashed lines, which agrees with the elastic responses of both FE models.

#### 3.2.1 Narrow end-post (Test 1)

The load-displacement curves for this test are shown in Figure 2a. Regarding the FE analyses, the behaviour was linear up to the shear force of 233 kN, which was 74% of the failure load of the fin-plate side. This failure occurred at the shear force of 313 kN, which was only 4% less than in the test (325 kN),

at the fin-plate connection side. This occurred by local buckling of the edge of the opening due to the high compressive stresses (Figure 3c) in a region that had reached its yield limit (Figure 3b). High stresses acted on the end-post, in tension in the upper one-third of the beam's depth and in compression in the lower one-third of the beam depth (Figure 3c).

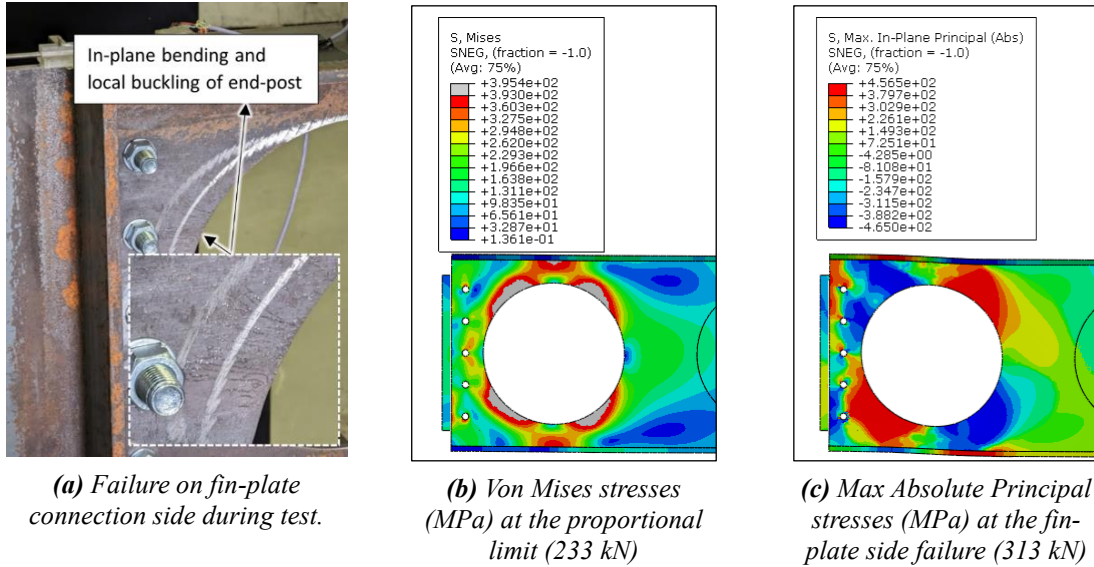


Figure 3. First failure at shear force of 313 kN at the fin-plate connection side (Test 1)

The model analysis continued following the loading protocol and the second failure occurred on the end-plate connection side at the shear force of 333 kN, close to the test failure load of 331 kN. The failure occurred by the formation of ‘plastic’ hinges due to the high Vierendeel bending moments at the first opening, next to the end-plate connection. This showed that failure of the end post next to the full depth end-plate connection did not occur.

3.2.2 Notched cellular beam with narrow end-post (Test 2)

This model analyses results agree well with the test results. The load-displacements curves are presented in Figure 2b. In the FE model, the failure occurred on the fin-plate connection side by buckling

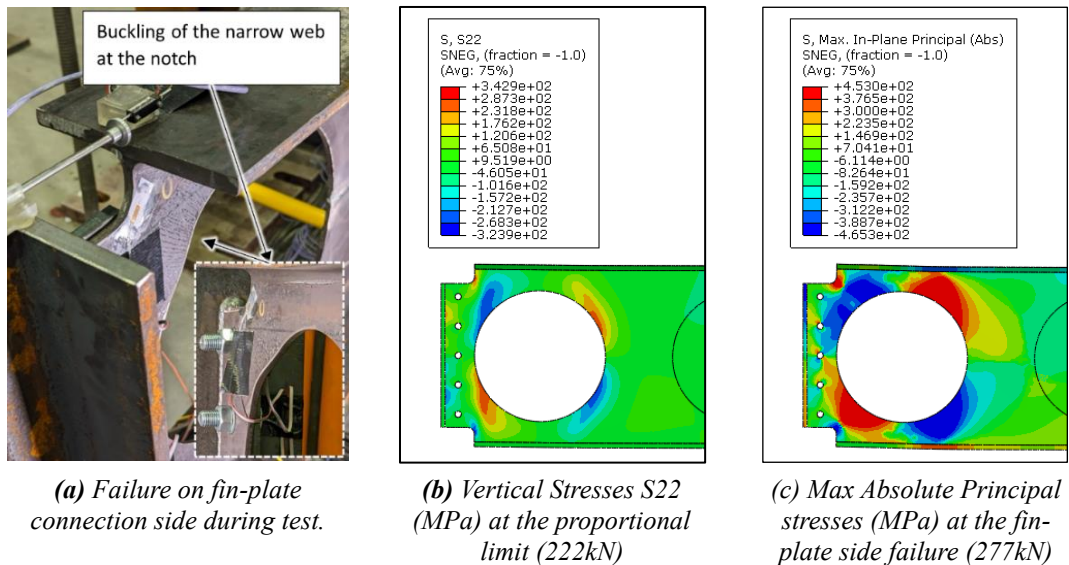


Figure 5. First failure at shear force of 277 kN at the fin-plate connection side (Test 2)

of the narrow web at the shear force of 277 kN, similar to the test (279 kN). The model's behaviour was linear up to 222 kN, which was 80% of the failure shear force at the fin-plate side. The high compressive vertical stresses at the top Tee next to the notch (Figures 5b) caused the buckling of the narrow web. Increased stress concentrations were also observed around the second and third bolts from the top of the 5-bolt connection at the failure load of 277 kN for this test (Fig. 5c).

The model analysis continued, following the test loading protocol, by increasing the load only on the end-plate side jack until failure in the FE model at the shear force of 288 kN. This was 3.4% less than in the test (298 kN). Similarly to the fin-plate side, the end-plate connection side failed by local buckling due to the high compressive vertical stresses S22 at the narrow web close to the notch.

### 3.2.3 Notched cellular beam with half-infill plate (Test 3)

The load-displacement curves for this test are shown in Figure 2c. Both the test and FE model behaviours were elastic up to the shear force of 282 kN. In the model analysis, the first failure was at the shear force of 417 kN that was 4.8% higher than in the test (398 kN). The model failed by buckling of the half-infill plate at the half-opening next to the fin-plate connection side, caused by the high compressive stresses (Figure 7c) in a region that had already partially yielded (Figure 7b). At the failure shear force, redistribution of stresses from the upper Tee in compression towards the bottom Tee in tension had developed (Figures 7c).

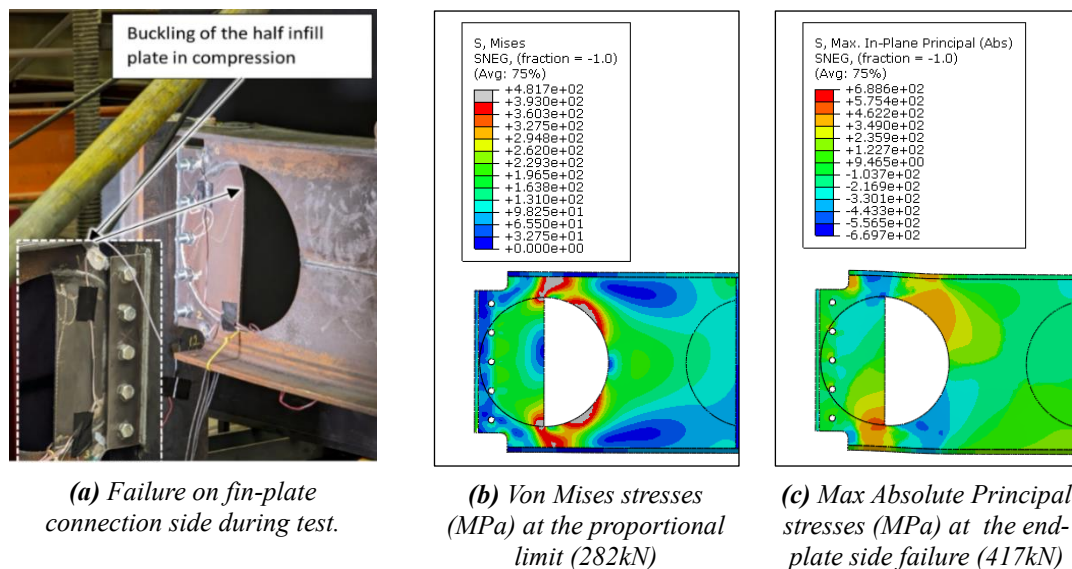


**Figure 7.** First failure at a shear force of 417 kN at the fin-plate connection side (Test 3)

The model analysis continued, and the second failure occurred on the end-plate side at the shear force of 431 kN, which was 3.4% higher than in the test. The end-plate connection side failed by Vierendeel bending of the half-opening, along with some transverse movement of the top flange. Hence, end-post failure did not occur.

### 3.2.4 Summary of the validation findings

The FEA results were in good agreement with the test results, having similar failure mechanisms and loads. Therefore, it is reasonable to assume that the test setup's modelling assumptions were accurate. Moreover, the two Abaqus solvers, Standard and Explicit, gave similar results. However, Standard solver provides a computationally more efficient solution, thus it will be employed for the follow up study of the failure of isolated cellular beam-to-columns connections.

**4. EXAMINATION OF ISOLATED CONNECTION SIDES**

To extend and further validate the previous study, each connection side was examined separately. This was done to confirm that failure loads and modes could be predicted well, especially for the second failure where prior loading and failure might have affected the outcome on the end-plate side. Additionally, a smaller model with just one beam-to-column connection is more computationally efficient and easier to assess. In total, eight isolated models were set up: the fin-plate and the end-plate sides separately for each of the three tests, plus two isolated models for a fourth model identical to Test 3, but without the notches. The validated isolated models are utilised in the parametric study where various practical end-post configurations are examined to understand their effect on failure load and mode.

**4.1. FE Modelling and Assumptions**

Identical modelling assumptions were made for all test specimens; the full models were set up as half span beams allowing for symmetry about mid-span. Although the original full test setup is not purely symmetric due to the different connections on either side, it is reasonable to ignore the small difference in the connection stiffnesses and model the isolated connection sides using axisymmetric boundary conditions, as shown in Figure 9. Apart from that, the rest of the boundary conditions and interactions were adopted from the full test models, including the lateral restraints at the mid-span. Regarding the loading and analysis steps, a reference load is applied to the beam over the stiffener until the failure occurs, which is achieved through a GMNIA using the Abaqus Standard Solver’s Buckling and Static Riks method analyses.

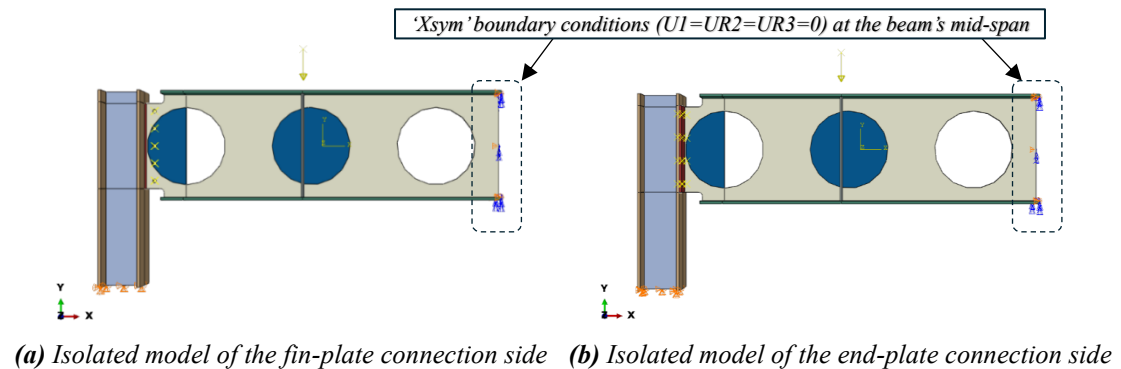


**Figure 9.** Isolating each connection side (Test 3).

All isolated models were compared against the full models. Results showed that the analyses of the isolated models presented similar behaviour to the full models. The good agreement also further validated the experimental results. The load–displacement curves showed that the isolated models and full models had similar stiffness, while the differences in the failure loads were less than 5%.

**Table 2.** Examined cases of isolated connection side models.

Models	Parameters												
	Opening diameter $h_o$ (mm)				End-post width $s_e$ (mm)					Notch length $X_{notch}$ (mm)			
	350	375	400	425	90	100	110	120	130	90	105	120	135
Test 1	✓	✓	✓	✓	✓	✓	✓	✓	✓	-	-	-	-
Test 2	✓	✓	✓	✓	✓	✓	✓	✓	✓	✓	✓	✓	✓
Test 3	✓	✓	✓	✓	-	-	-	-	-	✓	✓	✓	✓
Test 4	✓	✓	✓	✓	-	-	-	-	-	-	-	-	-

**4.2. Parametric Study**

In this section, a range of end-post configurations are examined for each of the eight test cases. These configurations varied depending on the values of the following three parameters: the opening diameter ( $h_o$ ), the end-post width ( $s_e$ ) and the notch length ( $X_{notch}$ ). The examined cases are presented in Table 2.

In total, 160 cases were analysed, including both end-post connection types. The following naming convention is used to refer to a specific modelling case: ‘T { test number } { connection side } – { h<sub>o</sub> value } – { s<sub>e</sub> value } – { X<sub>notch</sub> value }’, where the letters ‘E’ and ‘F’ are used for the end-plate and fin-plate connections respectively.

**4.2.1 Analysis of Test 1 results**

All end-plate side models failed by Vierendeel bending. The fin-plate side models failed by buckling of the narrow end-post, except for the cases of h<sub>o</sub> = 425mm and s<sub>e</sub> ≥ 100mm, where failure occurred by Vierendeel bending because the end-post was sufficiently wide to avoid its failure before the adjacent opening. In these cases, the compressive stresses near the end-post appeared farther away from it and closer to the upper Tee, causing the Vierendeel mechanism action at the first opening (Figure 10).

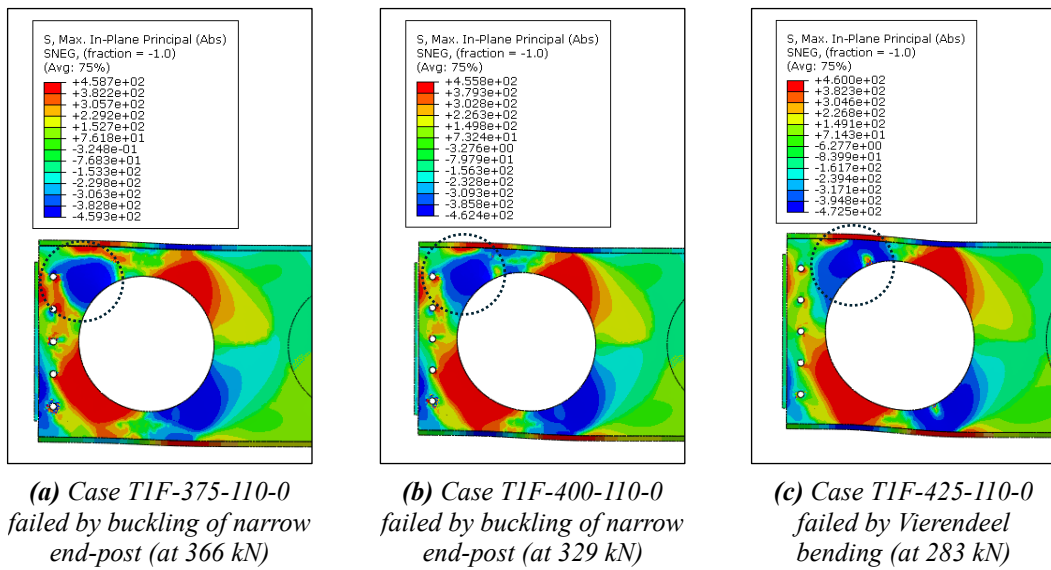


**Figure 10.** Max absolute principal stresses (MPa) at the fin-plate side failure (Test 1)

**4.2.2 Analysis of Test 2 results**

The 80 examined cases failed by buckling of the narrow end-post near the upper notch and displayed similar stress distribution patterns in the vicinity of the opening. The compressive stresses in the narrow

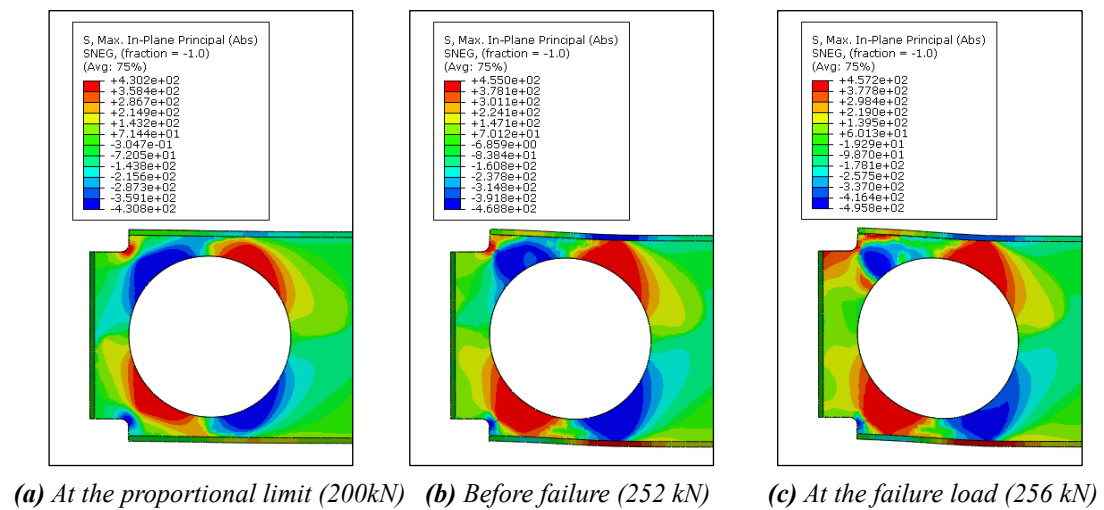


**Figure 11.** Max absolute principal stresses (MPa) evolution for case T2E-425-90-0

end-post caused the failure. Redistribution of stresses from the top Tee in compression to the bottom Tee in tension occurred after yielding and became more pronounced as buckling progressed (Fig. 11).

#### 4.2.3 Analysis of Test 3 results

The fin-plate side models failed by buckling of the infill plate next to the connection due to the high compressive stresses in the upper Tee near the notch. In most of those cases, the initial buckling of the half-infill plate was not critical, and a second ultimate failure followed in Vierendeel bending. As shown in Figure 12b, when the area between the notch corner and the web half-opening was sufficient in size, the end-post would resist the compressive stresses and would guide the failure to the first half-opening. The end-plate side models failed by Vierendeel bending, except for two cases, namely ‘T3E-425-3-135’ and ‘T3E-350-3-135’, where the failure occurred by buckling of the half-infill plate.

#### 4.2.4 Analysis of Test 4 results

Similar to the Test 3 cases, the fin-plate side models initially failed by buckling of the half-infill plate, followed by the failure mode in Vierendeel bending. All end-plate side models failed by Vierendeel bending. The stress distributions in the vicinity of the opening and in the end-post were similar to the Test 3 cases with Xnotch equal to 90mm (Figures 12a and 12b), indicating that a narrow notch does not have a significant effect on the end-post behaviour for both connection sides.

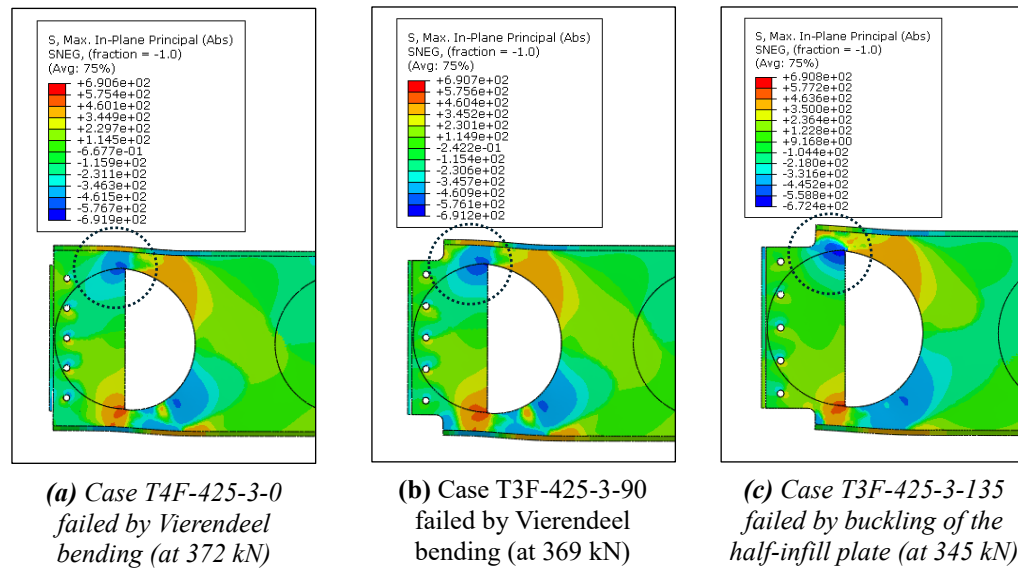


Figure 11. Max absolute principal stresses (MPa) at the fin-plate side failure (Tests 3 and 4)

The analyses results of the complete parametric study are available in an open repository on OSF: [https://osf.io/p3t68/?view\\_only=d5c63e893f7e4d8fb97034eba25474f0](https://osf.io/p3t68/?view_only=d5c63e893f7e4d8fb97034eba25474f0).

## 5. CONCLUSIONS FROM THE FE STUDY OF END-POSTS

Following the successful FE validation of the six connection tests presented in Tsavdaridis et al. (2024), a parametric study was carried out to investigate the end-post behaviour of a wider range of end-posts to cellular beams. The study involved 160 end-post configurations, taking into consideration current practice and design guides. The FE analyses results showed that:

- The end-plate connection strengthened the end-post, allowing it to resist higher shear loads than the respective fin-plate side. Moreover, the end-plate had a clear effect on the failure mode, as nearly all Test 1, 3 and 4 cases failed by Vierendeel bending at the first opening next to the end-post, which

is justified by the fact that the stiffer end-plate connection provided more stability to the end-post, and led to failure at the nearest web opening.

- Among the examined parameters, the results showed that the web opening diameter ( $h_o$ ) was dominant in determining the end-post shear resistance. Its effect on the failure mode was less critical, as the connection type primarily controlled the failure mechanism. The end-post width ( $s_e$ ) and the notch length ( $X_{\text{notch}}$ ) values had a smaller effect on the failure loads and modes.

- Stress contour plots revealed that the region in compression in the upper Tee close to the end-post is the one that mainly determines the failure; when it appears further away from the end-post, the failure will come by Vierendeel bending, else by buckling. Moreover, after yielding, stress is redistributed from that region in compression towards the neighbouring tension zones. .

To fully evaluate the effect of the connection type on the end-post failure mode, the effect of small end moments and other geometric parameters should be studied.

## 6. REFERENCES

- [1] ALTIFILLISCH, M.D., COOKE, B.R. AND TOPRAC, A.A. (1957) 'An investigation of open web expanded beams', *Welding Research*, 22(2).
- [2] BRITISH STANDARDS INSTITUTION (2024) 'Eurocode 3: Design of steel structures - Part 1-13: Beams with large web openings', BS EN 1993-1-13:2024.
- [3] CHUNG, K.F., LIU, C.H. AND KO, A.C.H. (2003) 'Steel beams with large web openings of various shapes and sizes: An empirical design method using a generalised moment-shear interaction curve', *Journal of Constructional Steel Research*, 59(9). Available at: [https://doi.org/10.1016/S0143-974X\(03\)00029-4](https://doi.org/10.1016/S0143-974X(03)00029-4).
- [4] CHUNG, K.F., LIU, T.C.H. AND KO, A.C.H. (2001) 'Investigation on Vierendeel mechanism in steel beams with circular web openings', *Journal of Constructional Steel Research*, 57(5). Available at: [https://doi.org/10.1016/S0143-974X\(00\)00035-3](https://doi.org/10.1016/S0143-974X(00)00035-3).
- [5] DASSAULT SYSTÈMES (2020) 'Abaqus 2020 Reference Library'. Available at: <https://help.3ds.com/2020x/>.
- [6] DASSAULT SYSTÈMES (2020) 'Abaqus/CAE 2020'. Available at: <https://www.3ds.com/products-services/simulia/products/abaqus/>.
- [7] FARES, S.S., COULSON, J. AND DINEHART, D.W. (2016) 'AISC 31 Design Guide: Castellated and Cellular Beam Design', American Institute of Steel Construction.
- [8] GRILO, L.F. ET AL. (2018) 'Design procedure for the web-post buckling of steel cellular beams', *Journal of Constructional Steel Research*, 148. Available at: <https://doi.org/10.1016/j.jcsr.2018.06.020>.
- [9] LAWSON, R.M. AND HICKS, S.J. (2011) 'Design of Composite Beams with Large Web Openings', SCI P355.
- [10] REDWOOD, R.G. (1973) 'Design of Beams with Web Holes' Canadian Steel Industries Construction Council.
- [11] REDWOOD, R.G. AND MCCUTCHEON, J.O. (1968) 'Beam tests with unreinforced web openings', *Journal of the Structural Division*, 94(1), pp. 1–17.
- [12] TSAVDARIDIS, K.D. ET AL. (2024) 'Cellular beam end-posts with two connection types, end notches and infill plates', *Journal of Constructional Steel Research*, 215, p. 108547. Available at: <https://doi.org/10.1016/J.JCSR.2024.108547>.
- [13] TSAVDARIDIS, K.D. AND D'MELLO, C. (2011) 'Web buckling study of the behaviour and strength of perforated steel beams with different novel web opening shapes', *Journal of Constructional Steel Research*, 67(10). Available at: <https://doi.org/10.1016/j.jcsr.2011.04.004>.
- [14] WARD, J.K. (1990) 'Design of composite and non-composite cellular beams', SCI Publication 100.